Ternary Phase Diagram of Dipalmitoyl-PC/Dilauroyl-PC/Cholesterol: Nanoscopic Domain Formation Driven by Cholesterol

Gerald W. Feigenson and Jeffrey T. Buboltz
Field of Biophysics, Biotechnology Building, Cornell University, Ithaca, New York 14853 USA

ABSTRACT A ternary phase diagram is proposed for the hydrated lamellar lipid mixture dipalmitoylphosphatidylcholine/dilauroylphosphatidylcholine/cholesterol (DPPC/DLPC/cholesterol) at room temperature. The entire composition space has been thoroughly mapped by complementary experimental techniques, revealing interesting phase behavior that has not been previously described. Confocal fluorescence microscopy shows a regime of coexisting DPPC-rich ordered and DLPC-rich fluid lamellar phases, having an upper boundary at apparently constant cholesterol mole fraction $\chi_{chol} \sim 0.16$. Fluorescence resonance energy transfer experiments confirm the identification and extent of this two-phase regime and, furthermore, reveal a 1-phase regime between $\chi_{chol} \sim 0.16$ and 0.25, consisting of ordered and fluid nanoscopic domains. Dipyrene-PC excimer/monomer measurements confirm the new regime between $\chi_{chol} \sim 0.16$ and 0.25 and also show that rigidly ordered phases seem to disappear around $\chi_{chol} \sim 0.25$. This study should be considered as a step toward a more complete understanding of lateral heterogeneity within biomembranes. Cholesterol may play a role in domain separation on the nanometer scale.

INTRODUCTION

The physical properties of biomembranes have intrigued researchers for many years. In this report, we focus on one particular aspect of these properties, the composition dependence of equilibrium phase behavior. Distinct, localized membrane environments could play an important role in nature, so the study of membrane biochemistry would be advanced by an improved understanding of the lateral heterogeneities that form within lamellar lipid mixtures. A composition-dependent phase diagram can serve as a starting point for modeling studies at the molecular level, and can therefore reveal the underlying physical properties that give rise to lateral heterogeneity. Here we describe a strategy for determining the phase diagram of a three-component lipid mixture. We then report interesting phase behavior, summarized on a ternary phase diagram, for the particular lipid mixture that we have studied, dipalmitoylphosphatidylcholine/dilauroylphosphatidylcholine/cholesterol (DPPC/DLPC/cholesterol).

The accumulated evidence for lateral heterogeneity is strong, in both biological membranes and experimental model mixtures. Observations made on real biomembranes indicate the presence of compositionally distinct membrane domains, especially in studies that are based on fluorescence microscopy or resistance to detergent solubilization (Brown and Rose, 1992; Thomas et al., 1994; Mayor and Maxfield, 1995; Edidin, 1997; Simons and Ikonen, 1997; Brown and London, 1998; Varma and Mayor, 1998; Sheets et al., 1999; Viola et al., 1999; Jacobson and Dietrich, 1999; Pralle et al., 2000; Schütz et al., 2000). In an effort to understand the molecular basis for detergent-insoluble domains, Xu and London (2000) have shown that, in binary model mixtures, tight packing of saturated lipid chains and certain sterols can be correlated with resistance to detergent insolubility. Other model studies have focused on a variety of two-component lipid mixtures (Marsh, 1990; Caffrey, 2000). In particular, the temperature dependence of DPPC/cholesterol mixtures has been studied by various spectroscopic and calorimetric methods (Ladbrooke et al., 1968; Estep et al., 1978; Mabrey et al., 1978; Rechtenwald and McConnell, 1981; Sankaram and Thompson, 1990a; Vist and Davis, 1990; Huang et al., 1993; Guo and Hamilton, 1995; McMullen and McElhaney, 1995).

A consistent result has been that lateral heterogeneities can be observed using a range of physical and chemical probes, even in simple two-component mixtures. Unfortunately, the spatial and temporal scales that characterize these heterogeneities have generally been poorly defined (reviewed by Edidin, 1997), and, therefore, quantitative descriptions of membrane lipid domains have remained elusive, as have their underlying physical origins.

Although model membrane studies offer the advantages of chemically well-defined mixtures, they generally have been limited by at least two factors. First, most systematic research has focused on two-component mixtures. It may well be that the study of more complex systems will reveal important properties that are not present in binary mixtures. Second, most analyses of model membrane phase behavior have been constrained to consider only classical first-order phase transitions. Experimental data have been interpreted to be consistent with this constraint, rather than to consider explanations based on other general models (e.g., non-ideal mixing or second-order transitions). Studies of ternary mixtures containing cholesterol have illustrated this interpretive limitation (Almeida et al., 1993; Silvius et al., 1996). For

Received for publication 13 November 2000 and in final form 23 March 2001.

Address reprint requests to Gerald W. Feigenson, Cornell Univ., 201 Biotechnology Bldg., Ithaca, NY 14853-2703. Tel.: 607-255-4744; Fax: 607-255-6249; E-mail: gwf3@cornell.edu.

0006-3495/01/06/2775/14 $2.00

example, Silvius and coworkers placed their results from infrared spectroscopy and fluorescence quenching on a classical ternary phase diagram. However, these experiments are sensitive to the local membrane environment only, so these data could reflect marked deviations from ideal mixing or higher order transitions in the absence of first-order phase separation.

An experimental strategy to establish the composition-dependent phase behavior in a model biomembrane mixture should observe at least three considerations. 1) The mixture chosen for study should be complex enough to mimic important features of phase behavior that could play a role in real biomembranes. 2) The experimental techniques should be complementary, so that several independent parameters are evaluated, each sensitive to either different physical properties or different spatial and temporal scales. 3) A large number of samples should be examined, thoroughly mapping the entire composition space, so that phase behavior will be revealed, whatever its nature and without regard to preconceptions.

Because phase behavior depends on the chemical nature and concentration of each mixture component, we note that the major lipids of mammalian plasma membranes are cholesterol, phosphatidylcholine (PC), sphingomyelin (Sph), phosphatidylethanolamine (PE), phosphatidylserine (PS), and lesser fractions of numerous other lipids (Devaux and Seigneuret, 1985; Zachowski, 1993). Associated proteins account for about 50 weight% of the membrane, with much of this protein extramembranal. Although membrane proteins can influence the lipid phases (Jähnig, 1981b; Epand, 1997), we do not consider these effects here. We plan to examine protein effects after the lipid phase behavior has been established.

As the subject of this study, we have chosen a three-component lipid mixture that can be expected to mimic some features of phase behavior in mammalian plasma membranes. Based on analyses of the outer leaflet of mammalian plasma membranes (Zachowski, 1993; Roelofsen and Op den Kamp, 1994), one such candidate mixture would be the ternary system Sph/palmitoyloleoylphosphatidylcholine(POPC)/cholesterol. (Because water and various ions are present, this is a pseudoternary system. We neglect any changes in water or ion content of the phases (Johann et al., 1996.) This mixture includes one lipid that forms an ordered phase in water at room temperature (Sph), one that forms a fluid phase in water (POPC), and the most abundant single chemical species in mammalian plasma membranes, cholesterol. However, to obtain the advantage of comparing a ternary phase diagram to the larger available literature of binary phase diagrams, it is reasonable to choose a ternary mixture for which the phase behavior has been examined in all three binary mixtures. DPPC/DLPC/cholesterol offers this advantage. Like Sph/POPC/cholesterol, DPPC/DLPC/cholesterol mixtures should manifest ordered, fluid, and coexistence phase regimes, as well as any cholesterol-rich phase behavior. Moreover, this ternary mixture has well-established phase behavior along the entire binary axis DPPC/DLPC (Van Dijck et al., 1977), and along both DPPC/cholesterol and DLPC/cholesterol axes in the regime of very high cholesterol mole fraction χ_{chol} (Huang et al., 1999).

Here we report that our study of DPPC/DLPC/cholesterol by complementary experimental techniques, together with a strategy of thoroughly mapping the entire composition space, has revealed interesting phase behavior that has not been previously described. Confocal fluorescence microscopy reveals a regime of coexisting DPPC- and DLPC-rich phases, having an upper boundary at apparently constant $\chi_{chol} \sim 0.16$. Fluorescence resonance energy transfer experiments confirm the identification and extent of this two-phase regime and, furthermore, reveal a one-phase regime between $\chi_{chol} \sim 0.16$ and 0.25, consisting of DPPC- and DLPC-rich "nanoscopic" domains: as DPPC content increases, the DPPC-rich domains increase in extent continuously but without macroscopic phase separation until the entire sample consists of an ordered DPPC-rich phase. Dipyrene-PC excimer/monomer measurements confirm the new regime between $\chi_{chol} \sim 0.16$ and 0.25 and also show that rigidly ordered phases seem to disappear around $\chi_{chol} \sim 0.25$. Overall, this study should be considered as a step toward a more complete understanding of lateral heterogeneity within biomembranes. In particular, we suggest a role for cholesterol in domain separation on the nanometer scale.

MATERIALS AND METHODS

Materials

Phospholipids were purchased from Avanti Polar Lipids, Inc. (Alabaster, AL) with the exception of the fluorescently labeled probes. The fluorescent probes 1,1′-dieicosanyl-3,3,3′,3′-tetramethylindocarbocyanine perchlorate (DiI-C20:0), 3,3′-dilinoleyloxacarbocyanine perchlorate (DiO-C18:2), and 1-hexadecanoyl-2-(4,4-difluoro-5,7-dimethyl-4-bora-3a,4a-diaza-s-indacene-3-pentanoyl)-*sn*-glycero-3-phosphocholine (Bodipy-PC) were obtained from Molecular Probes (Eugene, OR). The fluorescent probe 1,2-(1-pyrenenonanoyl)-*sn*-glycero-3-phosphocholine (dipyrene-PC) was synthesized as described in Hinderliter et al., (1994). Cholesterol was purchased from Nu Chek Prep (Elysian, MN). Purity of >99.5% was confirmed by thin-layer chromatography on washed, activated silica gel plates (Alltech, Deerfield, IL), developed with chloroform/methanol/water (65:25:4) for all phospholipids, chloroform/methanol (9:1) for DiI-C20:0 and DiO-C18:2, and with petroleum ether/diethyl ether/chloroform (7:3:3) for cholesterol analysis. Phospholipid stock solutions were quantitated by phosphate assay (Kingsley et al., 1979).

Confocal fluorescence microscopy of giant unilamellar vesicles

Giant unilamellar vesicles (GUVs) were prepared essentially according to Akashi et al., (1996), except that sample incubation was at ~50°C. Stock chloroform solutions of DLPC and DPPC contained 10 mol% DLPG or DPPG, respectively, because charged phospholipids are necessary to obtain GUVs by this method. PG was chosen to serve as the charged lipid because main transition temperatures are nearly identical for PG and PC having the

same acyl chains (Findlay and Barton, 1978). For visualization by confocal fluorescence microscopy (CFM), fluorescent probes were added to the lipid mixtures at a concentration of ~0.1 mol%. The aqueous buffer was 50 mM KCl, 5 mM Pipes, and 1 mM EDTA, pH 7.0. After incubation at 50°C for 10–20 h, samples were slowly (~1–2°C/h) cooled to room temperature. Image acquisition was carried out at ambient temperature, ~24°C. Harvested GUVs were placed on a no. 1 coverslip, then enclosed by a glass microscope slide within a ring of silicone high-vacuum grease, and allowed to settle for ~10 min, where they remained stationary over the course of the experiment.

CFM images were obtained with an MRC600 confocal microscope (Bio-Rad, Hercules, CA) at 488-nm excitation, with a 560-nm dichroic beamsplitter, and emission filters of 522/35BP for Bodipy-PC and 585LP for DiI-C20:0. The objective was 40× water immersion, numerical aperture 0.75. For three-dimensional image projection of a vesicle, z-scans in 1-μm increments were taken through the upper half of a GUV. These scans were then combined and color-merged using the software application NIH Image.

Fluorescence resonance energy transfer

Vesicles were prepared by injecting an ethanolic solution of the lipids into buffer, essentially as described by Batzri and Korn (1973). Stock chloroform solutions were measured into 75 × 100-mm glass tubes. A stock solution of DiO-C18:2/DiI-C20:0 ~1/4 in ethanol was added to each sample to give a DiO/PC ratio of ~1/1000. After mixing, solvent was evaporated under N_2 gas, followed by brief pumping under high vacuum. The dry lipid films were redissolved in 20 μL of ethanol and injected into vortexing buffer (200 mM KCl, 5 mM Pipes, 1 mM EDTA, pH 7.0) at 50°C. Each sample was then sealed under argon until the fluorescence measurement. Final PC aqueous concentration was 30 μM. Samples were then incubated at 42°C for 10–20 h, gradually cooled to room temperature (~23°C) over 24 h, and held at this temperature for another 12–24 h before measurement. Some samples were prepared by a different method, Rapid Solvent Exchange (Buboltz and Feigenson, 1999), and produced comparable results.

Fluorescence was measured with a Hitachi (San Jose, CA) 3010 spectrofluorimeter, exciting at 470 nm using a 470-nm interference filter and a 5-nm slit width. Emission was measured at 505 nm (DiO) and 568 nm (DiI), with a 10-nm slit width. Cuvet temperature was 23°C. The fluorescence ratio, F_{568}/F_{505}, was used as a measure of the energy transfer efficiency, rather than either the sensitized acceptor fluorescence F_{568} or the donor fluorescence F_{505} alone. Use of this ratio corrects the data for sample-to-sample variations in total lipid concentration.

To examine quantitatively whether reduced fluorescence resonance energy transfer (FRET) efficiency within a regime of coexisting ordered and fluid membrane phases is caused by differential probe partitioning (see Results), FRET profiles were fit to a simple probe partitioning model: Given a probe's overall concentration within the lipid mixture, its concentration within the coexisting phases will be determined by its partition coefficient, K_p. If the FRET profile follows a thermodynamic tie line, then, at any given composition within the two-phase region, the relative quantities of the coexisting phases will be determined by the Lever Rule. Therefore, we measured the fluorescence intensities (both F_{505} and F_{568}) as a function of the probe concentrations (χ_{DiO}, χ_{DiI}) within both of the coexisting phases, so that a FRET ratio could be computed for any given pair of probe K_p. In this way, we determined a unique K_p^{DiO}, K_p^{DiI} pair, which best fit the experimental FRET profile.

Dipyrene-PC excimer/monomer ratio

Samples were prepared by injection of ethanolic solutions as described above, except that dipyrene-PC was added to the ternary mixture at a ratio of ~1/1000 to PC. Excitation was at 340 nm using a 340-nm interference filter and a 3-nm slit width. Emission was measured at 398 nm (monomer) and 480 nm (excimer) with a 10-nm slit width. The ratio of these uncorrected fluorescence readings is referred to as excimer/monomer (E/M). Care was taken to minimize exposure of samples to air during incubation and during fluorescence measurement.

RESULTS AND DISCUSSION

Confocal fluorescence microscopy

In DPPC/DLPC GUVs at 25°C, coexisting DPPC-rich ordered and DLPC-rich fluid lamellar phases of macroscopic dimensions (greater than ~300 × 300 nm) can be reliably visualized by CFM (Korlach et al., 1999; see Bagatolli and Gratton, 2000, for a two-photon version of this experiment). For this purpose, we use two dyes with similar excitation maxima and significantly different emission maxima, and which partition differentially between the coexisting phases: DiI-C20:0, which favors DPPC-rich phases over coexisting fluid phases (Spink et al., 1990), and Bodipy-PC, which favors the fluid phase. These complementary probes produce clear visualizations of coexisting phases in GUV of DPPC/DLPC. Figure 1 illustrates the form of the data, showing Bodipy-PC fluorescence (*upper left*), DiI-C20:0 fluorescence (*upper right*), and the merged, colorized image below. Orange fluorescence from DiI-C20:0 identifies the DPPC-rich ordered phase, and green fluorescence from Bodipy-PC identifies the DLPC-rich fluid phase. A great advantage of using complementary dyes is that common artifacts, such as bound small vesicles or patches of additional lipid, can easily be recognized and therefore not interpreted as actual phase separation. Representative images from a systematic examination of GUVs prepared over a range of DPPC/DLPC/cholesterol compositions are shown in Fig. 2. In this and other experiments, sample compositions are described by a pair of numbers, the mole fraction of all of the lipid that is cholesterol (χ_{chol}) and the fraction of all of the PC that is DPPC (χ_{DPPC}^{PC}). GUV compositions were examined from $0.0 \leq \chi_{DPPC}^{PC} \leq 1.0$ and from $0.0 \leq \chi_{chol} \leq 0.40$.

Consider the data for $\chi_{chol} = 0$ shown as the bottom row of Fig. 2. Consistent with the published temperature–composition phase diagram for DPPC/DLPC (Van Dijck et al., 1977), uniform fluorescence for each dye is observed over the entire vesicle for $\chi_{DPPC}^{PC} < 0.3$ and $\chi_{DPPC}^{PC} > 0.85$, at 23°. As expected, coexistence of macroscopic ordered and fluid domains is evident for $0.3 < \chi_{DPPC}^{PC} < 0.85$. We briefly note that confocal fluorescence microscopy seems to be a good way to determine the connectivity of coexisting phases. For example, at $\chi_{chol} = 0.0$ the Bodipy-PC and C20:0DiI fluorescence images show the fluid phase to be continuous at $\chi_{DPPC}^{PC} = 0.3$ and 0.4, whereas only the ordered phase is continuous from $\chi_{DPPC}^{PC} = 0.5$ to 0.8.

As cholesterol is added to DPPC/DLPC mixtures, solidus and fluidus phase boundaries can be detected up to an overall cholesterol concentration $\chi_{chol} \sim 0.16$. However,

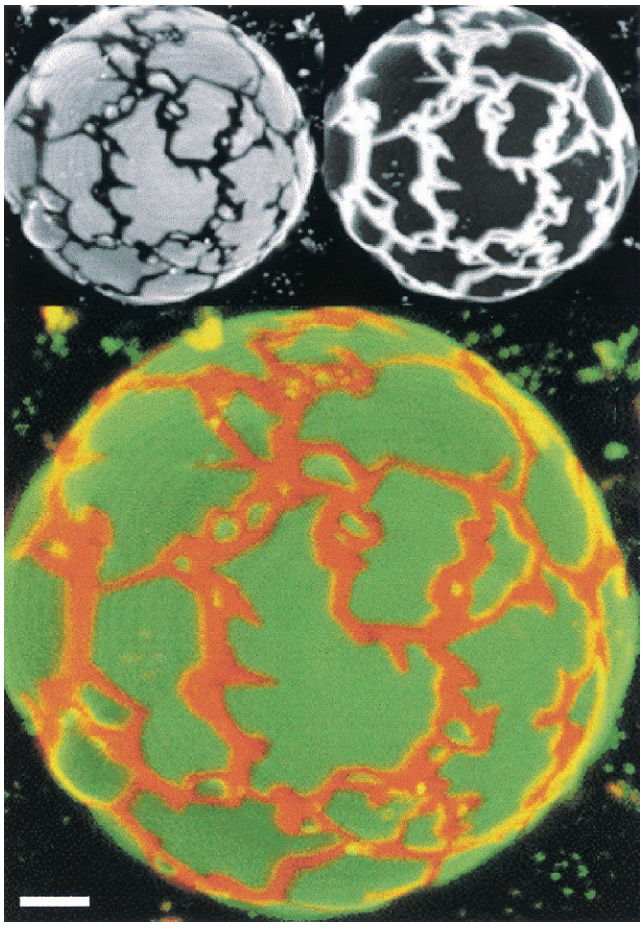

FIGURE 1 The principle of lipid phase identification, showing confocal fluorescence microscopy images of a GUV. The lipid composition of this GUV was DPPC/DLPC = 1/1, with DiI-C20:0 and Bodipy-PC dyes at mole fraction ~0.001. Excitation was at 488 nm. The upper right image is the fluorescence emission through a 585 nm LP filter, thus almost exclusively from DiI-C20:0. The upper left image is the emission through a 522 nm 35-nm BP filter, thus almost exclusively from Bodipy-PC. The bottom image is color-merged, using the public domain NIH Image program (developed at the U.S. National Institutes of Health and available on the Internet at http://rsb.info.nih.gov/nih.gov/nih-image/). The bar represents 5 μm.

precise location of these boundaries was not achieved due to the gradual appearance or disappearance of the minor phase as sample compositions were varied. Rather, for a given χ^{PC}_{DPPC}, the boundary was established by the lowest χ_{chol} above which only uniform fluorescence was observed, and below which coexisting phases were evident, in replicated, independent experiments. These data are summarized in Fig. 3.

Remarkable behavior was observed for the compositions $0.6 < \chi^{PC}_{DPPC} < 0.85$. In this range, coexistence of DPPC- and DLPC-rich macroscopic phases persists up to $\chi_{chol} \sim 0.16$, as seen in Fig. 3. However, at this critical cholesterol concentration, macroscopic phase coexistence is suddenly abolished. As χ_{chol} is gradually increased in increments of 0.003, visual detection of phase coexistence disappears abruptly at $\chi_{chol} = 0.16 \pm 0.003$. That is, for $0.6 < \chi^{PC}_{DPPC} < 0.85$, the phase boundary appears to be horizontal, with all samples prepared above $\chi_{chol} \sim 0.16$ showing uniform fluorescence.

This surprisingly abrupt disappearance of coexisting lamellar phases does not imply, however, that compositionally distinct (i.e., DPPC- and DLPC-rich) domains have suddenly been abolished on every spatial scale. Our inability to resolve any such domains by CFM implies only that the spatial scale of any such domains, should they exist, must be smaller than ~300 nm. Any such submicrometer-scale (i.e., nanoscopic) domains would be invisible by CFM, and their detection would require another technique.

Fluorescence resonance energy transfer

Pedersen et al. (1996) proposed a suitable method for detecting coexisting membrane domains near a first-order thermotropic phase transition. Two fluorescent probes were used, which must form an efficient donor–acceptor pair and also partition differentially between the phases.

Here we report that this method can be especially powerful in revealing the presence of both coexisting micrometer-scale and nanometer-scale membrane domains. For such a pair of probes, a regime of phase coexistence must be manifest as a regime of reduced FRET as the dyes become spatially separated. The fluorescent dyes DiI-C20:0 and DiO-C18:2 serve as a suitable pair of probes for our experiments. When a series of DPPC/DLPC/cholesterol samples are prepared, such that their compositions traverse a two-phase region, the measured FRET will pass through a marked regime of reduced efficiency (which we abbreviate as RRE) in a manner consistent with simple differential probe partitioning.

To illustrate this, two FRET profiles, containing RREs and traversing the two-phase region, have been fit with a simple probe-partition model, as shown in Fig. 4. At $\chi_{chol} = 0$ (Fig. 4, □), the RRE is fit best by $K_p^{DiO} = 8.0 \pm 0.5$; $K_p^{DiI} = 0.20 \pm 0.05$, with DiO-18:2 favoring the fluid-phase and DiI-20:0 favoring the ordered phase, as expected. Upon increasing the cholesterol concentration to just below the threshold for abolishing macroscopic phase coexistence, the differential partitioning seems to be but slightly reduced: the RRE at $\chi_{chol} = 0.15$ (Fig. 4, ○) is fit best by $K_p^{DiO} = 7.0 \pm 0.5$; $K_p^{DiI} = 0.3 \pm 0.05$.

Because the FRET profiles across the two-phase region are fit so well by this simple model, yielding K_p consistent with expectations, we interpret RREs as signifying demixing of DiI-C20:0 and DiO-C18:2 due to differential partitioning. With this in mind, consider Fig. 5, which shows an offset series of FRET profiles at increasing cholesterol concentrations. Each of these profiles shows a marked RRE. The boundaries of these regimes change

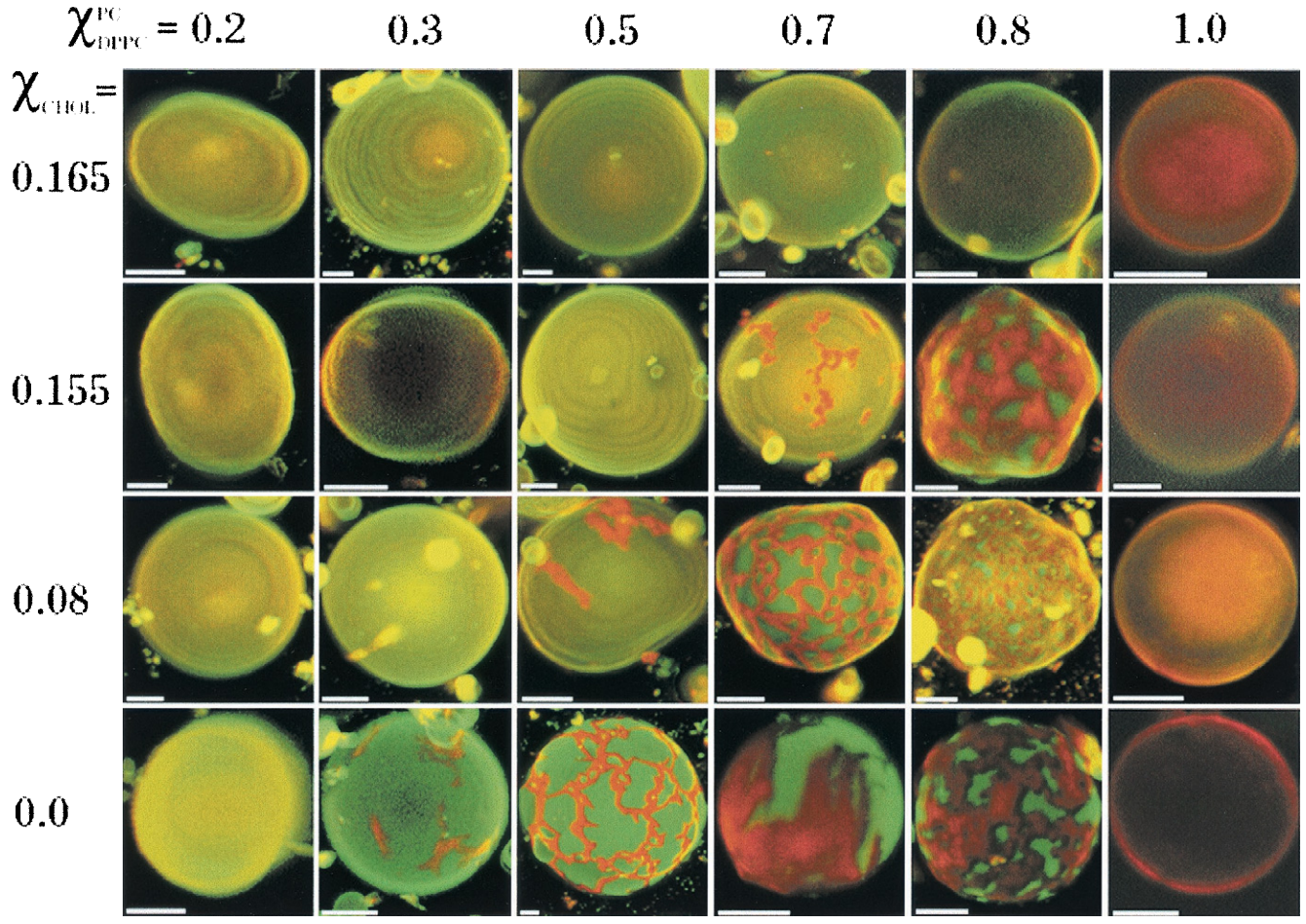

FIGURE 2 Composition dependence of phase behavior in giant unilamellar vesicles of DPPC/DLPC/cholesterol is visualized using confocal fluorescence microscopy. Each image is color-merged from the simultaneously collected fluorescence emission from DiI-C20:0 (*orange*) and Bodipy-PC (*green*), with both dyes at mole fraction ~0.001. Images were constructed from confocal microscopy z-scans in 1-μm increments. Coexisting fluid phases (*green*) and solid-like phases (*orange*) are observed over a range of compositions. This phase coexistence disappears abruptly at cholesterol mole fraction $\chi_{chol} \sim 0.16$. Fluorescence quantum yield of Bodipy-PC is low in mixtures with $\chi^{PC}_{DPPC} = 1.0$, so these uniform GUV appear to be depleted of green fluorescence. Bars are 5 μm. Temperature was 24°C.

smoothly with composition, with RREs persisting up to $\chi_{chol} \sim 0.25$. Apart from RREs, we have not tried to interpret any other features of our FRET profiles (e.g., either steep or more gradual χ^{PC}_{DPPC}-dependence of FRET outside these regimes). These features of the FRET profiles do not imply domain formation and could perhaps be the result of nonideal mixing of the probe molecules or probe orientation changes.

To reveal better any patterns in the FRET data, it is useful to view the entire data set together: a set of profiles corresponding to 18 values of χ_{chol}. Examining these in a two-dimensional (2D) stacked plot is problematic, however, due in part to compression of the ordinate data. Therefore, consider Fig. 6, a three-dimensional (3D) plot, which shows two views of an entire FRET data set up to $\chi_{chol} = 0.50$. Figure 6 *A* shows that the distinctive pattern of RRE extends from $\chi_{chol} = 0.0$ to ~0.25. Figure 6 *B* shows that this regime terminates abruptly at $\chi_{chol} \sim 0.26$. Although RREs are to be expected for $\chi_{chol} < \sim 0.16$, it is noteworthy to observe RREs for $\chi_{chol} > \sim 0.16$, because GUVs of this composition show no evidence of coexisting phases by CFM. However, this regime of reduced FRET efficiency ($\sim 0.16 < \chi_{chol} < \sim 0.25$; $\sim 0.6 < \chi^{PC}_{DPPC} < \sim 0.85$) is unmistakable when the FRET data are viewed in either 2D (Fig. 5) or 3D (Fig. 6). Therefore, we interpret this regime to be one of nanoscopic domain formation.

Finally, Fig. 6 *B* shows that, for all higher cholesterol concentrations that were examined ($\sim 0.25 < \chi_{chol} < \sim 0.5$), the FRET data are free of any RREs. Based on this observation we do not infer that other domain-forming regimes are absent from this large region of composition space, but only that none have been detected by this particular pair of DiO/DiI probes.

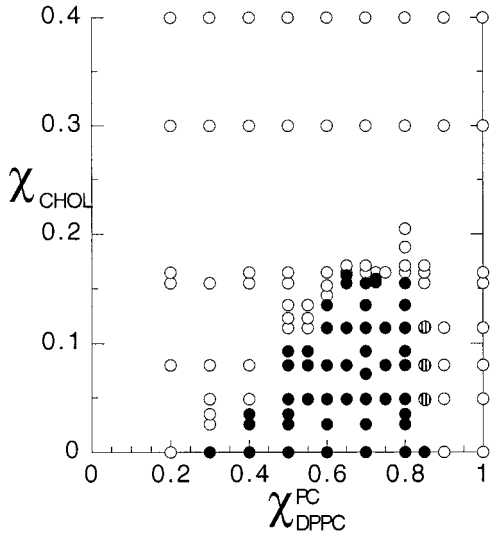

FIGURE 3 GUV images from confocal fluorescence microscopy plotted according to lipid composition show that phase coexistence disappears for $\chi_{chol} > 0.16$. Images of GUV composed of DPPC/DLPC/cholesterol obtained as in Fig. 1 are scored as showing uniform fluorescence (○), coexisting phases (●), or borderline (◍).

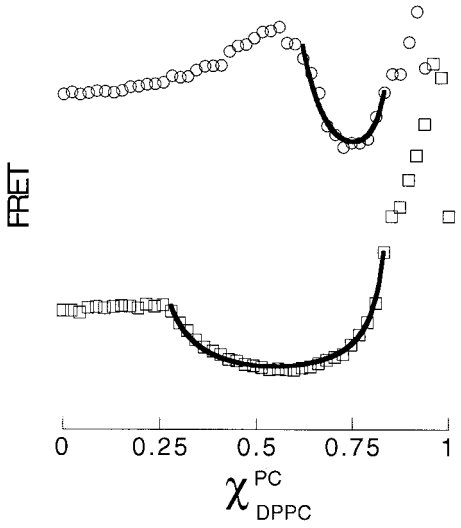

FIGURE 4 Regimes of reduced efficiency of fluorescence resonance energy transfer are fit by a simple model of probe partitioning between coexisting phases. Donor and acceptor probes were DiO-C18:2 and DiI-C20:0, respectively. Temperature was 23°C, excitation was at 470 nm, and the ratio of F_{568}/F_{505} was used to measure FRET in this and other figures. When fluid and ordered phases coexist, fluorescence resonance energy transfer between DiO-C18:2 and DiI-C20:0 is reduced by differential probe partitioning between the phases. Experimental profiles (*open symbols*) are shown together with best fits by a simple probe partitioning model (*lines*). For $\chi_{chol} = 0.0$ (□), the experimental data are best fit by $K_p^{DiO} = 8.0 \pm 0.5$; $K_p^{DiI} = 0.20 \pm 0.05$. For $\chi_{chol} = 0.15$ (○), the data are best fit by $K_p^{DiO} = 7.0 \pm 0.5$; $K_p^{DiI} = 0.3 \pm 0.05$.

Dipyrene-PC excimer/monomer ratio

Domain formation is not the only possible type of composition-dependent phase behavior. For this reason, we examined the behavior of DPPC/DLPC/cholesterol mixtures by a different method that is based on the properties of a dipyrene-PC probe. The intramolecular E/M ratio is sensitive to local molecular motion, order, and "free volume" (Vauhkonen et al., 1990). Dipyrene-PC offers good signal/noise (S/N) at low concentration, and its E/M ratio can change dramatically with the phase state of the bilayer. This is illustrated by Fig. 7, in which a series of offset E/M profiles are shown at increasing cholesterol concentrations. As χ^{PC}_{DPPC} increases, a precipitous drop in E/M at $\chi^{PC}_{DPPC} \sim 0.85$ signals the formation of an ordered lamellar phase.

Figure 8 plots dipyrene-PC E/M over the full range of lamellar phase compositions. The same data are shown from three alternative perspectives: Fig. 8 *B* is a 90° clockwise rotation of Fig. 8 *A*; Fig. 8 *C* is an expanded view of one region shown in Fig. 8 *B*. Consider Fig. 8 *B*. For $\chi^{PC}_{DPPC} \sim 1.0$, E/M is relatively constant (at the low value ~0.5) for $\chi_{chol} < 0.25$, and then increases rather steeply up to the highest χ_{chol} examined. Similarly, Sunamoto et al. (1980) observed low E/M for a dipyrene-PC probe in cholesterol-free gel phase bilayers of DPPC at 25°C, with an approximately three-fold increase in E/M upon mixing with cholesterol at $\chi_{chol} \sim 0.4$. These researchers also found an increase in E/M upon heating pure DPPC bilayers above the main transition temperature. Therefore, E/M is lowest in the DPPC-rich ordered lamellar phase (a rigid lattice inhibits excimer formation), higher in the fluid phase (a fluid lattice is more permissive for excimer formation), and highest in the fluid-ordered phase(s), which forms at high χ_{chol} (a fluid-ordered lattice favors the highest rate of excimer formation).

With this in mind, consider the remarkable wedge-shaped feature that is revealed clearly in Fig. 8 *C*. At high DPPC content, $\chi^{PC}_{DPPC} \sim 0.85$, this wedge-shaped region is bounded by $\sim 0.16 < \chi_{chol} < \sim 0.25$. At lower χ^{PC}_{DPPC}, the boundaries vary from $\chi_{chol} \sim 0.25$ at $\chi^{PC}_{DPPC} \sim 0.4$ to $\chi_{chol} \sim 0.16$ at $\chi^{PC}_{DPPC} \sim 0.7$. Given the observations summarized in the preceding paragraph, this region of locally-elevated E/M could indicate a composition regime that is fluid yet ordered. However, when $\chi_{chol} > 0.25$, Fig. 8 *B* illustrates that E/M increases smoothly with cholesterol concentration up to cholesterol saturation of the bilayer. This implies that any composition-dependent phase transitions that may occur at higher cholesterol concentrations are unlikely to be accompanied by sudden changes in either the acyl chain order or motional state of the membrane.

Spatial scales of membrane domains

The CFM images of coexisting membrane phases (Figs. 1 and 2) show that they are easily resolved by optical microscopy. Therefore, we can set a relatively firm minimum size

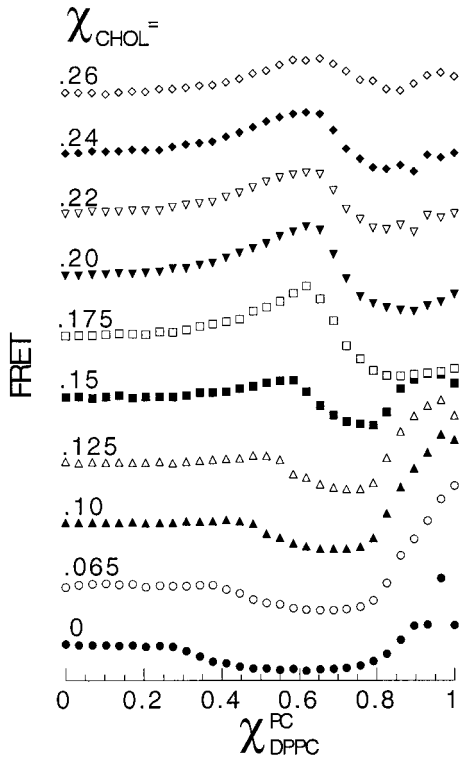

FIGURE 5 Regimes of reduced efficiency of FRET indicate lipid composition-dependent spatial separation of fluorescent donors from acceptors. Offset plots of fluorescence resonance energy transfer between DiO-C18:2 and DiI-C20:0 show RREs indicating coexisting membrane domains throughout the two-phase regime ($0 < \chi_{chol} < \sim 0.16$). RREs are also observed at higher cholesterol concentrations, throughout a regime of nanoscopic domain coexistence, $\sim 0.16 < \chi_{chol} < \sim 0.25$.

for these separated phase domains: $\sim 300 \times 300$ nm or $\sim$150,000 lipids, while noting that essentially all domains observed are actually much larger. This optical resolution limit could be reduced somewhat further with a more sophisticated image analysis (Kenworthy and Edidin, 1998; Schütz et al., 2000).

Membrane domains that cause RREs in FRET (Figs. 4–6) must also be greater than some minimum size for the probes to be photophysically separated. Assuming randomly distributed donors and acceptors, Wolber and Hudson (1979) analyzed the distance dependence of FRET in the bilayer phase. More recently, Zimet et al. (1995) considered a similar system, in which a fluorescently-labeled lipid acceptor is effectively excluded by protein from an area surrounding a protein-bound donor. In this case, very little reduction in FRET occurs for protein diameters smaller than the Förster distance (R_0), whereas nearly maximal reduction occurs for diameters $>4R_0$. For FRET between DiO and DiI, we estimate R_0 to be $\sim$50–60 Å, based on DiO-DiI quenching curves and on the calculated spectral overlap integral for the fluorophors. R_0, the distance at which FRET is 50% of maximum (Förster, 1948), was determined in two ways. First, following Fung and Stryer (1978) and Wolber and Hudson (1979), the quenching of DiO as a function of DiI concentration in the bilayer yielded a value $R_0 \sim 80$ Å if only DiI in one leaflet quenches, or $R_0 \sim 60$ Å if DiI quenches equally from both leaflets (data not shown). Second, following Förster (1948) and computing the spectral overlap integral, $R_0 \sim 50$ Å. So, we can set a minimum domain diameter on the order of $R_0 \sim 50-60$ Å, which would be composed of $\sim$40–60 lipids. Note that this minimum size is comparable to the maximum possible cluster size for nonideal mixing without phase separation (Huang and Feigenson, 1993). If the domain size is larger than $\sim$50–60 Å, then RRE would be detected in FRET experiments using a donor and acceptor pair having an even larger R_0. In contrast, to detect smaller domains by FRET, a less efficient donor and acceptor pair should be chosen.

To evaluate lateral heterogeneity on even smaller spatial scales, a technique is needed having an extremely short and well-defined scale of distance dependence. One such technique is fluorescence quenching by spin-labels (London and Feigenson, 1981). Fluorescent probes of a variety of types can be quenched when they are within $\sim$10 Å of a nitroxide free radical. Thus, fluorescence quenching experiments (Silvius et al., 1996; Ahmed et al., 1997; Xu and London, 2000) are sensitive to very small separations between fluorophor and quencher, perhaps only 1–2 lipids (i.e., smallest-scale heterogeneities). Information at this spatial scale is important to studies of lateral heterogeneity, but it should be emphasized that the results of such experiments should not be taken as diagnostic of first-order phase separation.

Finally, a brief comment regarding the temporal scales of membrane domains is warranted. The FRET-based strategy for domain detection must average any lateral heterogeneities on the timescale of the DiO/DiI lifetimes. These are on the order of 10^{-9} s, whereas nearest-neighbor lipid exchange occurs on a timescale of 10^{-7} s. For this reason, we can say nothing of the characteristic lifetimes of nanoscopic domains. However, we can report that the macroscopic phase domains observed by fluorescence microscopy persist for at least an hour at 24°C, our longest continuous observation time. This can be compared with the recent reports by Schütz et al. (2000) that micrometer-scale domains persist for minutes in the plasma membrane of muscle cells, and by Dietrich et al. (2001) that GUV composed of Sph/DOPC/cholesterol show similar persistence of fluid but ordered macroscopic domains.

Ternary phase diagram

As a summary description, we have placed all of the results above on a triangular diagram, Fig. 9, which describes the observed phase behavior as a function of composition. Each region in this ternary phase diagram is now discussed.

A *DLPC-rich fluid lamellar phase, L_α.* This region has the following properties characteristic of an L_α phase. 1)

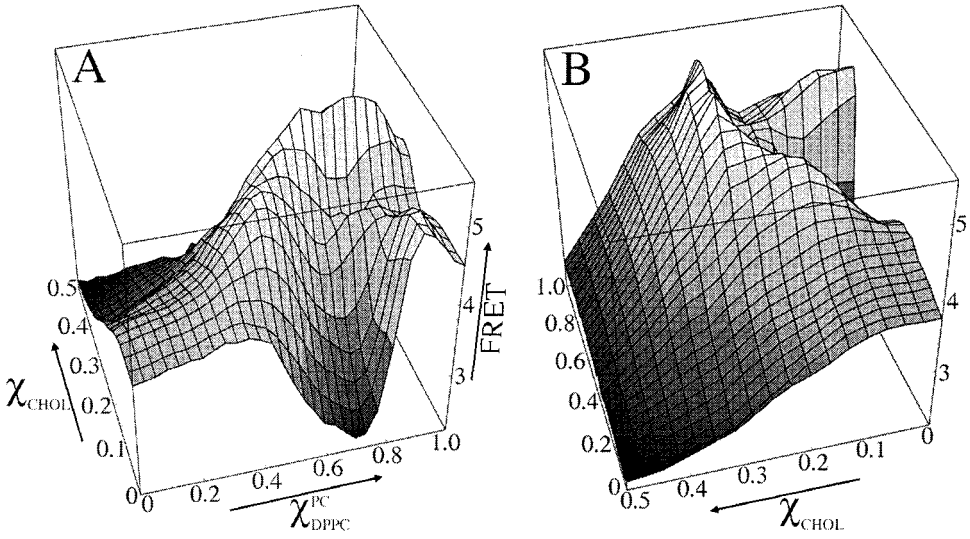

FIGURE 6 3D Views of FRET data, as a function of composition, reveal the characteristic patterns that reflect phase behavior. χ_{chol} ranges from 0.0 to 0.505, χ^{PC}_{DPPC} from 0.0 to 1.0. (*B*) is a 90° counter-clockwise rotation of (*A*). The regime of reduced energy transfer between DiO-C18:2 and DiI-C20:0, characteristic of coexisting membrane domains, is seen from $\chi_{chol} = 0.0$ to ~0.26. FRET then decreases monotonically for all higher χ_{chol}, at all values of χ^{PC}_{DPPC}. Data shown correspond to 600 independently prepared samples, at 23°C. Data scatter was reduced by three-point smoothing in both χ_{chol} and χ^{PC}_{DPPC} coordinate-spaces.

The translational diffusion coefficient of DiI-C20:0 is $\sim 3 \times 10^{-8}$ cm^2s^{-1} (Korlach et al., 1999). 2) E/M values are near those for pure DLPC hydrated fluid lamellae. 3) The fluid-preferring probes DiO-C18:2 and Bodipy-PC partition preferentially into this phase, whereas DiI-C20:0 partitions out of this phase.

B *Coexisting L_α and DPPC-rich ordered phases*. This assignment is based on several observations. 1) CFM shows separated macroscopic phase domains, and the expected probe partitioning behavior: DiI-C20:0 preferring the DPPC-rich ordered phase and BODIPY-PC the DLPC-rich fluid. 2) Within this region, FRET data are fit by a simple model of differential probe partitioning, with K_p values consistent with coexisting DLPC- and DPPC-rich phases. 3) D_T analysis of DiI-C20:0 yields two components, a fast one characteristic of diffusion in a fluid bilayer and a slower one characteristic of diffusion in ordered bilayers (Korlach et al., 1999). 4) L_α and DPPC-rich phase coexistence is quantitatively consistent, at both the fluidus and solidus boundaries, with the well-established L_α and L_β coexistence for $\chi_{chol} = 0$ (Van Dijck et al., 1977; Buboltz and Feigenson, 2000). Note that, because the upper boundary of this region is effectively horizontal, a small change in χ_{chol} acts as a switch between one- and two-phase regimes. Moreover, because both the upper and lower boundaries are horizontal, it may well be that all the thermodynamic tie lines in region B are horizontal. If so, then cholesterol must partition equally well into both the fluid and ordered phases.

C *DPPC-rich ordered phase*. E/M values are ~0.5 up to $\chi_{chol} \sim 0.25$, characteristic of a rigid ordered phase. CFM images are uniform. At $\chi^{PC}_{DPPC} = 1.0$, this is the $L_{\beta'}$ phase, an ordered phase with acyl chains tilted relative to the bilayer normal. However, there must be a transition between the $L_{\beta'}$ and L_β phases in this region, because the chain tilt characteristic of pure DPPC is abolished by the presence of low concentrations of cholesterol (Hui and He, 1983).

D *A single phase that changes continuously from a DPPC-rich ordered phase at the C/D boundary to a fluid-ordered phase at the D/E boundary*. According to CFM, this is a one-phase region, but RREs in FRET indicate differential probe partitioning, consistent with DLPC-rich (L_{02}) and DPPC-rich domains. Region D is part of the wedge-shaped region of locally elevated E/M seen in Fig. 8 *C*. The boundaries are defined by the loss of macroscopic phase coexistence at $\chi_{chol} \sim 0.16$, the rise in E/M at $\chi_{chol} \sim 0.16$, the abrupt drop in E/M at $\chi_{chol} \sim 0.25$, and the RRE boundaries at $\chi^{PC}_{DPPC} = \sim 0.62$ and 0.85. The high value of E/M throughout region D implies that the dipyrene-PC probe favors the fluid-ordered domains, although we have not attempted to determine its partition coefficient. It seems likely that, starting from the D/E boundary and increasing the DPPC concentration, the first nanoscale domains that form are probably "rigid-ordered-like" within a less rigid lattice. In contrast, starting from the C/D boundary and decreasing the DPPC concentration, the nanoscale domains that first start to form would be "fluid-ordered-like" within a more rigid lattice.

E *L_{02}, a fluid-ordered phase*. This region, as well as region D, is demarcated by a region of locally elevated E/M values seen in Fig. 8 *C*, suggesting a fluid-ordered phase.

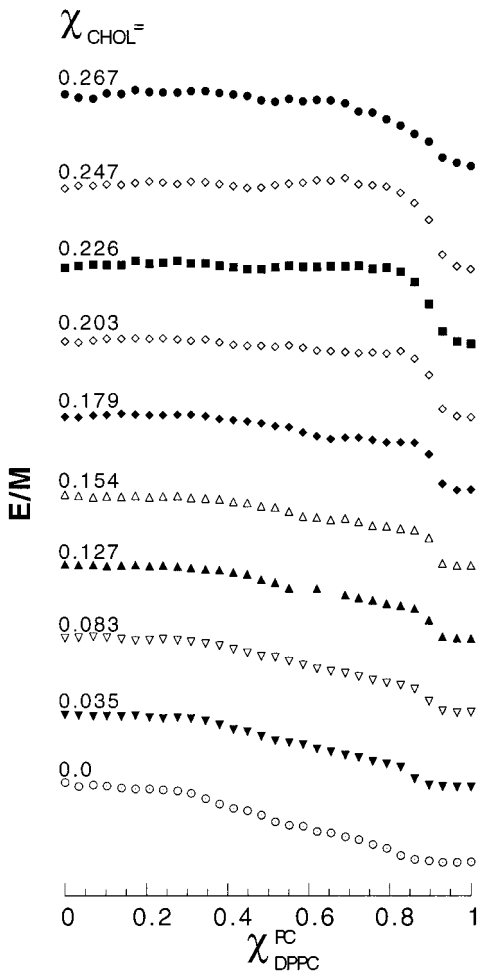

FIGURE 7 Excimer/monomer ratios of a dipyrene-PC probe drop to markedly low values in the rigid ordered phase at $\chi^{PC}_{DPPC} \sim 0.85$. F_{480}/F_{398} is used as a measure of E/M, in this and the following figure. Offset E/M profiles as a function of χ^{PC}_{DPPC} are stacked at increasing values of χ_{chol}. Up to $\chi_{chol} \sim 0.25$, E/M falls to ~0.5 at χ^{PC}_{DPPC} ~0.85, indicating a rigid-ordered phase. Samples at ~0.001 mole fraction probe were prepared by ethanol injection at 50°C, followed by slow cooling to room temperature.

We have not established precisely where region A ends and region E begins.

F *L_{01}, a fluid-ordered phase*. At least a portion of the lower boundary of F is at $\chi_{chol} \sim 0.25$ where E/M begins a smooth rise that continues all the way to $\chi_{chol} = 0.66$, the maximum cholesterol concentration that can be accommodated within DLPC/DPPC bilayers (Huang et al., 1999). We have not yet established the boundary between region F and region E. There might be a continuous transition between L_{02} and L_{01}, based on the nearly seamless change in E/M between these regimes. At high cholesterol content, the properties of this phase change little between the extremes in composition: D_T is 3×10^{-9} cm^2s^{-1} at $\chi_{chol} = 0.60$, $\chi^{PC}_{DPPC} = 0.0$ as compared with 1.5×10^{-9} cm^2s^{-1} at $\chi_{chol} = 0.60$, $\chi^{PC}_{DPPC} = 1.0$ (Korlach et al., 1999).

G *Coexisting crystalline cholesterol and a cholesterol-saturated lamellar phase*. In this regime, all cholesterol in excess of $\chi_{chol} = 0.66$ spontaneously phase separates to form crystals of cholesterol monohydrate (Huang et al., 1999).

Continuous phase transitions

In region D of our ternary phase diagram, the phases at the boundaries are different but do not separately coexist. In this region, addition of DPPC to compositions along the D/E boundary causes a continuous change of the phase, with the transition complete at the C/D boundary. Therefore, this transition is not first-order. Such transitions are variously termed second-order, higher order, or order–disorder transitions (Denbigh, 1981) or continuous transitions.

We are not the first to argue that continuous phase transitions occur in bilayer lipid mixtures containing cholesterol. Jähnig (1981a,b) considered that, in certain PC/cholesterol mixtures, the latent heat associated with the main (i.e., gel–fluid) transition decreases with increasing cholesterol content and ultimately disappears at a critical cholesterol concentration, $\chi_{chol} \sim 0.2$. Moreover, fluctuations in order parameter are maximal at $\chi_{chol} \sim 0.2$, as is lateral compressibility. According to Jähnig's theoretical treatment, the particular value of this critical cholesterol concentration depends upon the cross-sectional areas of phospholipid and cholesterol, and the coherence length of phospholipid interactions. In this connection, it is interesting to note that Blume and Hillmann (1986) reported that bilayers and monolayers of dimyristoylphosphatidic acid/cholesterol have a critical point at $\chi_{chol} \sim 0.12$, as indicated by light scattering.

In other liquid crystalline mixtures, higher-order transitions have been described for smectic-A to hexatic-B (Huang et al., 1989), smectic-A to smectic-C (Huang and Lien, 1985), for an aqueous equimolar mixture of 1-palmitoyllysoPC/dipalmitoylphosphatidylethanolamine (Checchetti et al., 1996), for DPPC (Mitaku et al., 1983), and for dimyristoylPC, distearoylPC and their bilayer mixtures (Sugár et al., 1999).

Studies of higher-order transitions have been an exciting experimental and theoretical topic in condensed matter physics for many years (see reviews by Strandburg, 1988; Dash, 1999). Indeed, the second-order thermotropic transitions of copper–zinc mixtures (β-brass) were the subject of active study more than 60 years ago (Jones and Sykes, 1937). Comparisons may even be drawn between our proposed phase diagram and the broader literature. For example, because the chemical potential of cholesterol is a function of its mole fraction, χ_{chol} could be viewed as a surrogate thermodynamic field variable. Given this point of view, one feature of our tentative phase diagram, the termination of a locus of second-order transitions (D/E boundary) at a first-order coexistence curve (region B boundary), is

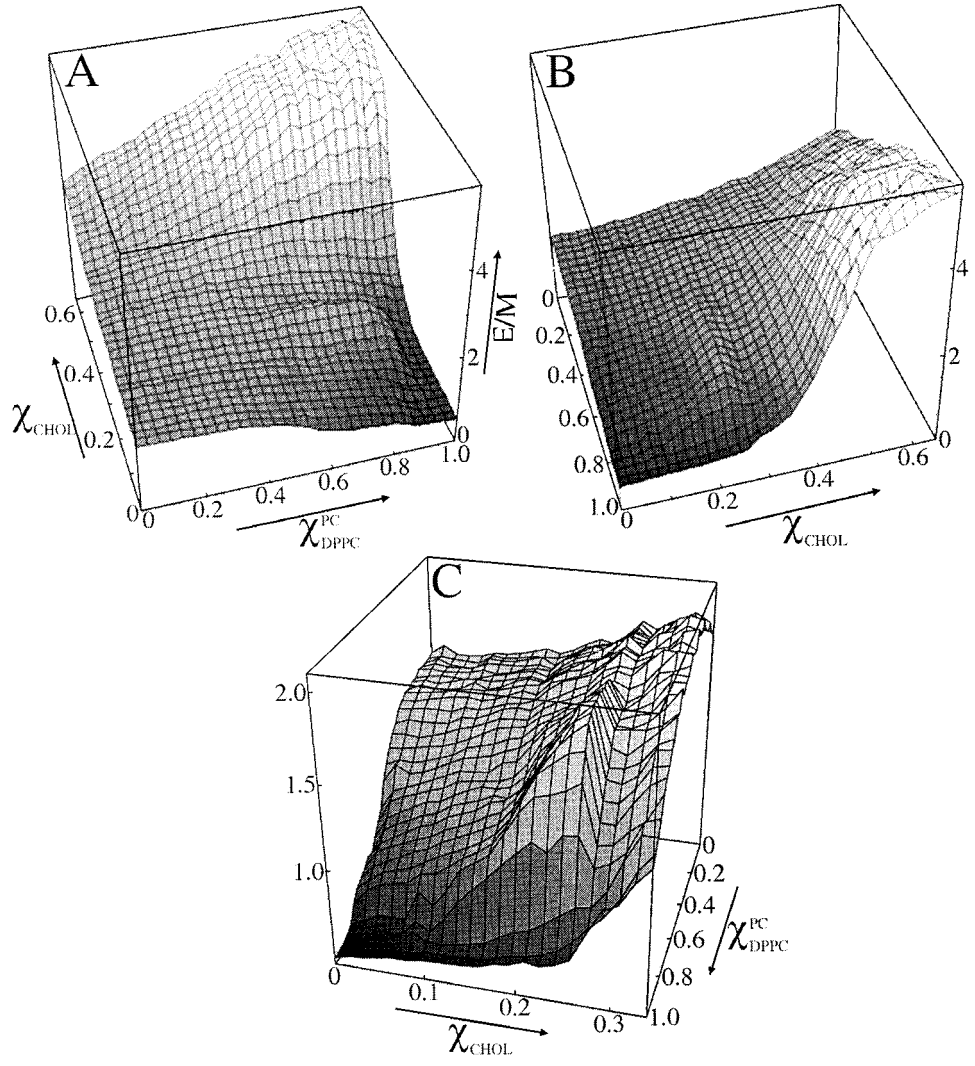

FIGURE 8 3D Views of E/M data, as a function of composition, reveal the patterns that reflect phase behavior. χ_{chol} ranges from 0.0 to 0.65, χ^{PC}_{DPPC} ranges from 0.0 to 1.0. (*B*) is a 90° clockwise rotation of (*A*). Plots reveal a region of locally elevated E/M, consistent with distinctive phase behavior phase (see "wedge" feature in each image). (*C*) an expanded view to show the wedge feature more clearly. The wedge of elevated E/M terminates abruptly at $\chi_{chol} \sim 0.25$. The low E/M values characteristic of a DPPC-rich ordered phase, front edge of (*B*), begin to rise at $\chi_{chol} \sim 0.25$, indicating a fluid-ordered phase. Data shown correspond to 990 independently prepared samples, at 23°C.

reminiscent of the thermotropic phase behavior in ^{4}He-^{3}He mixtures (Isihara, 1991). Moreover, in terms of this view, a distinctive feature of our phase diagram, the pronounced flatness of the coexistence curve near the critical point (i.e., $\chi_{chol} \sim 0.16$), may simply reflect the effective two-dimensionality of the DPPC/DLPC/cholesterol system (Rowlinson and Widom, 1989).

Molecular-level model

Now we speculate about the molecular interactions that may characterize DPPC/DLPC/cholesterol mixtures and the physical origin of these interactions.

In an earlier Monte Carlo study (Huang and Feigenson, 1999), Huang suggested that a dominant feature of phospholipid–cholesterol mixing is that the largely nonpolar cross-section of cholesterol must be shielded from contact with bulk water by neighboring phospholipid headgroups. Indeed, this requirement is reflected in a well-defined feature of our ternary phase diagram, the phase boundary at $\chi_{chol} = 0.66$ (Huang et al., 1999). This is the maximum cholesterol concentration for these bilayer mixtures, above which all additional cholesterol precipitates as the monohydrate crystal. Throughout the remaining discussion, we will elaborate on the role that phospholipid–cholesterol shielding could play at lower values of χ_{chol}, as we describe our provisional model for

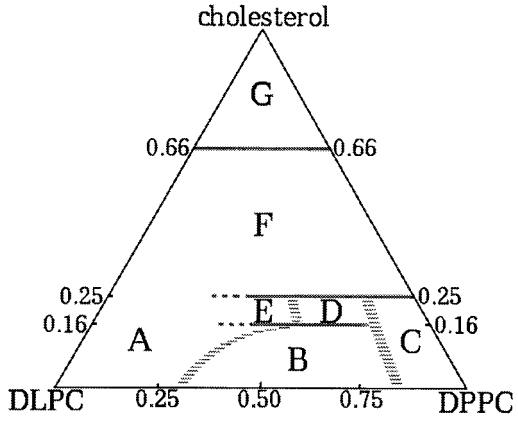

FIGURE 9 Ternary phase diagram for DPPC/DLPC/cholesterol, at 24°C. Each vertex represents a pure component in excess buffer. The numbers labeling the DLPC–DPPC axis correspond to χ^{PC}_{DPPC}, whereas the numbers labeling the PC–cholesterol axes correspond to χ_{chol} and indicate the values associated with various horizontal phase boundaries. To find the location in the diagram that corresponds to a given lipid composition, find the intersection of the χ^{PC}_{DPPC}-line (connects the cholesterol vertex to the appropriate point on the DLPC-DPPC axis) and the χ_{chol}-line (a horizontal line corresponding to the appropriate cholesterol mole fraction). The labeled regions of the diagram, described in more detail in the text, are: *A*, DLPC-rich fluid lamellar phase; *B*, coexisting fluid lamellar phase and DPPC-rich ordered phase; *C*, DPPC-rich ordered phase; *D*, a single phase that changes continuously from a rigid ordered phase at the *C/D* boundary to a fluid-ordered phase at the *D/E* boundary; *E*, a fluid-ordered phase; *F*, a fluid-ordered phase different from *E*; *G*, coexisting crystalline cholesterol monohydrate and a cholesterol-saturated lamellar phase. This phase diagram in entirely phenomenological, derived from confocal fluorescence microscopy, fluorescence resonance energy transfer, and fluorescence excimer/monomer ratios. Since the composition-space does not reflect other system components (i.e., water, buffer and ions), this diagram should be considered as a pseudo-ternary phase diagram (see Introduction).

composition-dependent phase behavior in DPPC/DLPC/cholesterol mixtures.

First we focus on the regime of coexisting DPPC-rich ordered and DLPC-rich fluid lamellar phases (region B, Fig. 9), noting that the addition of cholesterol up to mole fraction $\chi_{chol} \sim 0.16$ has a relatively modest effect on the phase boundaries. Cholesterol addition from $\chi_{chol} = 0.0$ to 0.16 does shift the fluidus boundary from ~0.3 to ~0.6, but hardly shifts the solidus, as seen by CFM (Fig. 3), FRET (Fig. 5), and E/M (Fig. 7). Furthermore, calorimetric measurements from many different laboratories are in agreement that the gel–fluid phase transition is only modestly influenced by cholesterol at low concentrations. For binary DPPC/cholesterol mixtures, the gel–fluid transition is somewhat broadened, by about 1°C, and shifted, also by about 1°C, when χ_{chol} is increased from 0.0 to ~0.15 (Mabrey et al., 1978; Estep et al., 1978; Huang et al., 1993; McMullen and McElhaney, 1995).

According to our provisional model (and consistent with calorimetric data), when cholesterol is dilute, its nonpolar cross section can be shielded from water by very slight rearrangements of the nearest-neighbor PC headgroups. However, when every PC headgroup in the mixture has accommodated one nearest-neighbor cholesterol, then any additional cholesterol must suffer some exposure to water unless the lattice changes. Each PC would have a single cholesterol nearest-neighbor when the cholesterols have between 5 and 6 PC nearest-neighbors, depending upon lattice details. This critical cholesterol concentration corresponds to $\chi_{chol} \sim 0.143–0.167$.

Therefore, we propose that the fluid bilayer lattice undergoes a phase transition at $\chi_{chol} \sim 0.16$ to provide shielding of additional cholesterol from water. The lattice could rearrange either by collapsing the cross-sectional area of the acyl chains, by expanding the cross-sectional area of the headgroups, or both. Because the dipyrene-PC probe experiences an environment of increased acyl chain order above $\chi_{chol} \sim 0.16$, we propose that the fluid lattice rearranges with a sharp reduction in the cross-sectional area of the PC acyl chains. Each PC headgroup would then have a greater capacity to shield neighboring cholesterols from bulk water. As an example, consider that a PC that occupies 70 Å^2 in the L_α phase would occupy about 30 Å^2 less upon switching to all-*trans* acyl chains. This is nearly equal to the estimated 37-Å^2 cross-sectional area of cholesterol (Small, 1986). Further characterization of this putative chain-ordering transition at $\chi_{chol} \sim 0.16$ would require measurements of the acyl chain order parameter over a large range of compositions. However, this physical picture is consistent with the well-known cholesterol-induced increase in phospholipid acyl chain order parameter, and the so-called "condensing effect" (Leathes, 1925; Demel et al., 1967; Stockton and Smith, 1976; Vist and Davis, 1990).

But why should a transition of fluid-phase acyl chains to smaller cross-sectional area be coupled to the disappearance of macroscopic phase coexistence? FRET indicates that compositionally distinct domains persist well above $\chi_{chol} \sim 0.16$, even though macroscopic phases cannot be resolved by CFM. We speculate that the DPPC-rich ordered domains interact more favorably with the L_{02} phase (i.e., are "wetted" better) than with the more chain-disordered L_α phase, resulting in a dramatically reduced interfacial free energy. This is consistent with the general principle that interfacial tension vanishes when approaching a critical point (Rowlinson and Widom, 1989).

What happens if the cholesterol concentration increases further? The wedge-shaped region in Fig. 8 is sharply bounded at $\chi_{chol} \sim 0.25$, with the locally-elevated E/M characteristic of regions D and E abruptly dropping back down to a lower value at this cholesterol concentration. This suggests that the disappearance of the L_{02} phase is due to its inability to accommodate more cholesterol. Just above $\chi_{chol} \sim 0.25$, E/M begins to rise again, for all χ^{PC}_{DPPC}, and FRET begins a monotonic decrease (Fig. 6). Because $\chi_{chol} = 0.25$ corresponds to exactly 3 PC per cholesterol, we speculate that, at $\chi_{chol} = 0.25$, each cholesterol is sur-

rounded by exactly six all-*trans* acyl chains. The further addition of cholesterol would cause the free energy of this lattice to rise steeply, because a different lattice of PC headgroups would be necessary to shield any additional cholesterols from water. Such a headgroup reorientation would actually increase the area available for each acyl chain and for the additional cholesterol. Experiments sensitive to order parameter might yield evidence of these changes.

Other published studies of the ordered DPPC-rich phase are consistent with a key role for phospholipid-cholesterol shielding. At 22°C, with $\chi_{DPPC}^{PC} = 1.0$ and $\chi_{chol} = 0.0$, the DPPC-rich phase is the chain-tilted $L_{\beta'}$ phase (Tardieu, 1973). Wide-angle x-ray diffraction indicates that addition of cholesterol to the $L_{\beta'}$ phase results in a change of chain packing from orthorhombic to hexagonal (McIntosh, 1978), and low-angle diffraction shows a loss of chain tilt and a dramatic increase in interlamellar repeat distances (Hui and He, 1983). These lattice changes (and perhaps others) enable each cholesterol to be accommodated in the ordered DPPC-rich lattice up to $\chi_{chol} \sim 0.25$, or 3 PC per cholesterol.

According to our CFM studies of GUV, the Bodipy-PC and DiI-C20:0 probes were uniformly distributed throughout the DPPC-rich region. It should be noted, however, that these probes have not been selected for their ability to distinguish between coexisting DPPC-rich phases. Other researchers studying DPPC/cholesterol have interpreted spectroscopic changes that begin at $\chi_{chol} \sim 0.08$ and continue to $\chi_{chol} \sim 0.25$ as indicating the separation of a cholesterol-rich phase (Recktenwald and McConnell, 1981; Ipsen et al., 1987; Sankaram and Thompson, 1990a,b; Vist and Davis, 1990; Risbo et al., 1995). ^{13}C-NMR studies (Huang et al., 1993; Guo and Hamilton, 1995) have shown that, just beyond $\chi_{chol} \sim 0.06-0.08$, a narrowed component appears in the spectrum of *sn*2-carbonyl-labeled DPPC. This narrowed component has been interpreted as a change in conformation of the *sn*2 carbonyl, to approximately the magic angle ($\theta \approx 55°$), together with fast axial reorientation (Wittebort et al., 1982). In a pure phospholipid, this sharp component corresponds to the appearance of the fluid L_α phase, so the interpretation of the DPPC/cholesterol results has been that a new, cholesterol-rich "liquid–gel" phase (also termed the L_0 or β phase) has appeared. However, to rationalize observed line broadening in the supposed two-phase region, Huang et al. (1993) suggested that the data could indicate molecular exchange between coexisting domains on the order of ~100 lipids. Therefore, we would emphasize that our failure to observe coexisting DPPC-rich phases by CFM might be due to non-optimal probes, nanoscopic phase-domain scales, or both.

Finally, we note that McConnell and coworkers (Keller et al., 2000) have used monolayer studies of phospholipid/cholesterol mixtures at relatively low film pressures to propose that stoichiometric "condensed complexes" of 2 phospholipids/1 cholesterol form, by a cooperative mass action mechanism, in lipid bilayers. Apparently, the experimental conditions used for these monolayer studies are sensitive to formation of this 2/1 complex, but not to the cholesterol-induced phase changes that we observe in bilayers at $\chi_{chol} = 0.16$ and 0.25.

Implications and considerations

The system we have studied, DPPC/DLPC/cholesterol at 22°C, is not the best model for a mammalian plasma membrane. Now that we have established the basic features of this ternary phase diagram, studies of a better model, Sph/POPC/cholesterol at various temperatures, are underway.

In region D of our proposed ternary phase diagram, a phase transition occurs without macroscopic phase separation. We refer to this as a region of "continuous phase transition," having thermodynamic characteristics that require further study. For example, spatial correlation lengths should be evaluated throughout this region (e.g., by neutron scattering) and Monte Carlo simulations should be pursued in an effort to reproduce this hypothesized phase behavior based on a well-defined molecular-level model. All the regions of our proposed phase diagram must be characterized further (e.g., in terms of diffusion coefficient, order parameter, packing, and motional details). The insights thus provided will inform molecular dynamics calculations and Monte Carlo simulations.

One implication of the studies reported here is that multicomponent lipid mixtures are capable of a rich variety of phase behavior, including the coexistence of chemically distinct membrane environments. Regardless of whether these domains are manifest as either coexisting phases or as a single nanocomposite phase, it would be interesting to know how other components redistribute between these membrane environments (e.g., into ordered domains, fluid domains, or at domain boundaries). In general, we would like to understand the partitioning behavior of various membrane proteins, gangliosides, and lipid species. For example, consider the protein–protein interactions that are early events in signaling pathways (Incardona and Eaton, 2000). Are all such interactions to be understood purely in terms of protein–protein contacts? Or might there be groups of proteins that share similar partitioning behavior, being concentrated in certain types of lipid domains or at domain interfaces?

In this study, we have not addressed the issue of overall phase behavior in real mammalian plasma membranes. However, if there are coexisting ordered and fluid environments in mammalian plasma membranes, then membrane-bound molecules will partition between these environments and will be either concentrated with, or isolated from, certain other membrane-bound molecules. In addition, the diffusion of membrane-bound molecules will reflect the connectivity of these membrane environments. Therefore,

our understanding of membrane biochemistry will be greatly informed by any fundamental advances in our understanding of lateral heterogeneity within biomembranes.

Based on the arguments presented earlier, we suggest that cholesterol could serve to ramify coexisting phases, creating "nanocomposite" phases, (e.g., region D of Fig. 9). A highly ramified system of membrane environments would enhance the partitioning and diffusion kinetics of membrane components, so the biochemical implications of such a nanoscopic phase seem considerable. Perhaps these nanocomposite phases are related to "membrane rafts," cholesterol- and sphingomyelin-rich plasma membrane domains having characteristic protein content (Simons and Ikonen, 1997). If so, then perhaps raft terminology will need to be expanded: in region D, the isolated domains vary from rigid-ordered-like within a less rigid environment, to fluid-ordered-like within a more rigid environment. For $\chi_{chol} > 0.25$, no more rigid-ordered phase exists at any DPPC concentration. Any nanoscale domains that might exist with $\chi_{chol} > 0.25$ must be fundamentally different from those detected in region D.

This work was supported by National Science Foundation Grant MCB-0077630. The authors acknowledge the Donors of the Petroleum Research Fund, administered by the American Chemical Society, for partial support of this research. The authors would like to thank B. Widom for helpful discussions.

REFERENCES

Ahmed, S. N., D. A. Brown, and E. London. 1997. On the origin of sphingolipid/cholesterol-rich detergent-insoluble cell membranes: physiological concentrations of cholesterol and sphingolipid induce formation of a detergent-insoluble, liquid-ordered lipid phase in model membranes. *Biochemistry.* 36:10944–10953.

Akashi, K.-I., H. Miyata, H. Itoh, and K. Kinosita, Jr. 1996. Preparation of giant liposomes in physiological conditions and their characterization under an optical microscope. *Biophys. J.* 71:3242–3250.

Almeida, P. F. F., W. L. C. Vaz, and T. E. Thompson. 1993. Percolation and diffusion in three-component lipid bilayers: effect of cholesterol on an equimolar mixture of two phosphatidylcholines. *Biophys. J.* 64: 399–412.

Bagatolli, L. A., and E. Gratton. 2000. Two-photon fluorescence microscopy of coexisting lipid domains in giant unilamellar vesicles of binary phospholipid mixtures. *Biophys. J.* 78:290–305.

Batzri, S., and E. D. Korn. 1973. Single bilayer liposomes prepared without sonication. *Biochim. Biophys. Acta.* 298:1015–1019.

Blume, A., and M. Hillmann. 1986. Dimyristoylphosphatidic acid/cholesterol bilayers. *Eur. Biophys. J.* 13:343–353.

Brown, D. A., and E. London. 1998. Structure and origin of ordered lipid domains in biological membranes. *J. Membr. Biol.* 164:103–114.

Brown, D. A., and J. K. Rose. 1992. Sorting of GPI-anchored proteins to glycolipid-enriched membrane subdomains during transport to the apical cell surface. *Cell.* 68:533–544.

Buboltz, J. T., and G. W. Feigenson. 1999. A novel strategy for the preparation of liposomes: rapid solvent exchange. *Biochim. Biophys. Acta.* 1417:232–245.

Buboltz, J. T., and G. W. Feigenson. 2000. Detection of coexisting bilayer gel and fluid phases by equilibrium surface pressure analysis. *Langmuir.* 16:3606–3611.

Caffrey, M. 2000. The Lipid Data Bank. http://www.ldb.chemistry.ohio-state.edu.

Checchetti, A., A. Golemme, G. Chidichimo, C. LaRosa, D. Grasso, and P. W. Westerman. 1996. Effect of 1-palmitoyl lysophosphatidylcholine on phase properties of 1,2-dipalmitoyl phosphatidylethanolamine: a thermodynamic and NMR study. *Chem. Phys. Lipids.* 82:147–162.

Dash, J. G. 1999. History of the search for continuous melting. *Rev. Mod. Phys.* 71:1737–1743.

Demel, R. A., L. L. M. van Deenen, and B. A. Pethica. 1967. Monolayer interactions of phospholipids and cholesterol. *Biochim. Biophys. Acta.* 135:11–19.

Denbigh, K. 1981. The Principles of Chemical Equilibrium. 4th ed., Cambridge Univ. Press, Cambridge, U.K. 207–212.

Devaux, P. F., and M. Seigneuret. 1985. Specificity of lipid–protein interaction as determined by spectroscopic techniques. *Biochim. Biophys. Acta.* 822:63–125.

Dietrich, C., L. A. Bagatolli, Z. N. Volovyk, N. L. Thompson, M. Levi, K. Jacobson, and E. Gratton. 2001. Lipid rafts reconstituted in model membranes. *Biophys. J.* 80:1417–1428.

Edidin, M. 1997. Lipid microdomains in cell surface membranes. *Curr. Opin. Struct. Biol.* 7:528–532.

Epand, R. M. 1997. Modulation of lipid polymorphism by peptides. *Curr. Top. Membr.* 44:237–252.

Estep, T. N., D. B. Mountcastle, R. L. Biltonen, and T. E. Thompson. 1978. Studies on the anomalous thermotropic behavior of aqueous dispersions of dipalmitoylphosphatidylcholine-cholesterol mixtures. *Biochemistry.* 17:1984–1989.

Findlay, E. J., and P. G. Barton. 1978. Phase behavior of synthetic phosphatidylglycerols and binary mixtures with phosphatidylcholines in the presence and absence of calcium ions. *Biochemistry.* 17:2400–2405.

Förster, T. 1948. Zwischenmolekulare energiewanderung und fluoreszenz. *Ann. Physik.* 2:55–75.

Fung, B. K.-K., and L. Stryer. 1978. Surface density determination in membranes by fluorescence energy transfer. *Biochemistry.* 17: 5241–5248.

Guo, W., and J. A. Hamilton. 1995. A multinuclear solid-state NMR study of phospholipid–cholesterol interactions. Dipalmitoylphosphatidylcholine-cholesterol binary system. *Biochemistry.* 34:14174–14184.

Hinderliter, A. K., J. Huang, and G. W. Feigenson. 1994. Detection of phase separation in fluid phosphatidylserine/phosphatidylcholine mixtures. *Biophys. J.* 67:1906–1911.

Huang, C. C., and S. C. Lien. 1985. Effect of the smectic-A temperature range on the behavior of the smectic-A–smectic-C transition. *Phys. Rev. A.* 31:2621–2627.

Huang, C. C., G. Nounesis, R. Geer, J. W. Goodby, and D. Guillon. 1989. Calorimetric study of the smectic-A–hexatic-B phase transition of a liquid–crystal binary mixture. *Phys. Rev. A.* 39:3741–3744.

Huang, J., and G. W. Feigenson. 1993. Monte Carlo simulation of lipid mixtures: finding phase separation. *Biophys. J.* 65:1788–1794.

Huang, J., and G. W. Feigenson. 1999. A microscopic interaction model of maximum solubility of cholesterol in lipid bilayers. *Biophys. J.* 76: 2142–2157.

Huang, J., J. T. Buboltz, and G. W. Feigenson. 1999. Maximum solubility of cholesterol in phosphatidylcholine and phosphatidylethanolamine bilayers. *Biochim. Biophys. Acta.* 1417:89–100.

Huang, T.-H., C. W. B. Lee, S. K. Das Gupta, and R. G. Griffin. 1993. A ^{13}C and ^{2}H nuclear magnetic resonance study of phosphatidylcholine/cholesterol interactions: characterization of liquid–gel phases. *Biochemistry.* 32:13277–13287.

Hui, S. W., and N.-B. He. 1983. Molecular organization in cholesterol–lecithin bilayers by x-ray and electron diffraction measurements. *Biochemistry.* 22:1159–1164.

Incardona, J. P., and S. Eaton. 2000. Cholesterol in signal transduction. *Curr. Opin. Cell Biol.* 12:193–203.

Ipsen, J. H., G. Karlstrom, O. G. Mouritsen, H. Wennerstrom, and M. J. Zuckermann. 1987. Phase equilibria in the phosphatidylcholine–cholesterol system. *Biochim. Biophys. Acta.* 905: 162–172.

Isihara, A. 1991. Condensed Matter Physics. Oxford Univ. Press, New York, 277.

Jacobson, K., and C. Dietrich. 1999. Looking at rafts? *Trends Cell. Biol.* 9:87–91.

Jähnig, F. 1981a. Critical effects from lipid–protein interaction in membranes. I. Theoretical description. *Biophys. J.* 36:329–345.

Jähnig, F. 1981b. Critical effects from lipid–protein interaction in membranes. II. Interpretation of experimental results. *Biophys. J.* 36: 347–357.

Johann, C., P. Garidel, L. Mennicke, and D. Blume. 1996. New approaches to the simulation of heat-capacity curves and phase diagrams of pseudobinary phospholipid mixtures. *Biophys. J.* 71:3215–3228.

Jones, F. W., and C. Sykes. 1937. The superlattice in β brass. *Proc. Roy. Soc.* 161:440–446.

Keller, S. L., A. R. Radhakrishan, and H. M. McConnell. 2000. Saturated phospholipids with high melting temperatures form complexes with cholesterol in monolayers. *J. Phys. Chem. B.* 104:7522–7527.

Kenworthy, A. K., and M. Edidin. 1998. Distribution of a GPI-anchored protein at the apical surface of MDCK cells examined at a resolution of $<$100 Angstroms using imaging fluorescence resonance energy transfer. *J. Cell Biol.* 142:69–84.

Kingsley, P. B., and G. W. Feigenson. 1979. The synthesis of a perdeuterated phospholipid: 1,2-dimyristoyl-*sn*-glycero-3-phosphocholine-d_{72}. *Chem. Phys. Lipids.* 24:135–147.

Korlach, J., P. Schwille, W. W. Webb, and G. W. Feigenson. 1999. Characterization of lipid bilayer phases by confocal microscopy and fluorescence correlation spectroscopy. *Proc. Nat. Acad. Sci. U.S.A.* 96:8461–8466.

Ladbrooke, B. D., R. M. Williams, and D. Chapman. 1968. Studies on lecithin–cholesterol interactions by differential scanning calorimetry and x-ray diffraction. *Biochim. Biophys. Acta.* 150:333–340.

Leathes, J. B. 1925. Role of fats in vital phenomena. *Lancet.* 208:853–856.

London, E., and G. W. Feigenson. 1981. Fluorescence quenching in model membranes. 1. Characterization of quenching caused by a spin-labeled phospholipid. *Biochemistry.* 20:1932–1938.

Mabrey, S., P. L. Mateo, and J. M. Sturtevant. 1978. High-sensitivity scanning calorimetric study of mixtures of cholesterol with dimyristoyl- and dipalmitoyl-phosphatidylcholines. *Biochemistry.* 17:2464–2468.

Marsh, D. 1990. Handbook of Lipid Bilayers. CRC Press, Boca Raton, FL.

Mayor, S., and F. R. Maxfield. 1995. Insolubility and redistribution of GPI-anchored proteins at the cell surface after detergent treatment. *Mol. Biol. Cell.* 6:929–944.

McIntosh, T. J. 1978. The effect of cholesterol on the structure of phosphatidylcholine bilayers. *Biochim. Biophys. Acta.* 513:43–58.

McMullen, T. P. W., and R. N. McElhaney. 1995. New aspects of the interaction of cholesterol with dipalmitoylphosphatidylcholine bilayers as revealed by high-sensitivity differential scanning calorimetry. *Biochim. Biophys. Acta.* 1234:90–98.

Mitaku, S., T. Jippo, and R. Kataoka. 1983. Thermodynamic properties of the lipid bilayer transition. *Biophys. J.* 42:137–144.

Pedersen, S., K. Jorgensen, T. R. Baekmark, and O. G. Mouritsen. 1996. Indirect evidence for lipid domain formation in the transition region of phospholipid bilayers by two-probe fluorescence energy transfer. *Biophys. J.* 71:554–560.

Pralle, A., P. Keller, E.-L. Florin, K. Simons, and J. K. H. Hörber. 2000. Sphingolipid-cholesterol rafts diffuse as small entities in the plasma membrane of mammalian cells. *J. Cell Biol.* 148:997–1008.

Rechtenwald, D. J., and H. M. McConnell. 1981. Phase equilibria in binary mixtures of phosphatidylcholine and cholesterol. *Biochemistry.* 20: 4505–4510.

Risbo, J., M. Sperotto, and O. G. Mouritsen. 1995. Theory of phase equilibria and critical mixing points in binary lipid membranes. *J. Chem. Phys.* 103:3643–3656.

Roelofsen, B., and J. A. F. Op den Kamp. 1994. Plasma membrane phospholipid asymmetry and its maintenance: the human erythrocyte as a model. *Curr. Top. Membr.* 40:7–46.

Rowlinson, J. S., and B. Widom. 1989. Molecular Theory of Capillarity. Chap. 9. Clarendon Press, Oxford, U.K. 249–306.

Sankaram, M. B., and T. E. Thompson. 1990a. Interaction of cholesterol with various glycerophospholipids and sphingomyelin. *Biochemistry.* 29:10670–10675.

Sankaram, M. B., and T. E. Thompson. 1990b. Modulation of phospholipid acyl chain order by cholesterol. A solid-state ^{2}H nuclear magnetic resonance study. *Biochemistry.* 29:10676–10684.

Schütz, G. J., G. Kada, V. Ph. Pastushenko, and H. Schindler. 2000. Properties of lipid microdomains in a muscle cell membrane visualized by single molecule microscopy. *EMBO J.* 19:892–901.

Sheets, E. D., D. Holowka, and B. Baird. 1999. Critical role for cholesterol in Lyn-mediated tyrosine phosphorylation of FcεRI and their association with detergent-resistant membranes. *J. Cell Biol.* 145:877–887.

Silvius, J. R., D. del Giudice, and M. Lafleur. 1996. Cholesterol at different bilayer concentrations can promote or antagonize lateral segregation of phospholipids of differing chain length. *Biochemistry.* 35:15198–15208.

Simons, K., and E. Ikonen. 1997. Functional rafts in cell membranes. *Nature.* 387:569–572.

Small, D. M. 1986. Sterols and sterol esters. *In* The Physical Chemistry of Lipids. Plenum Press, New York. 407.

Spink, C. H., M. D. Yeager, and G. W. Feigenson. 1990. Partitioning behavior of indocarbocyanine probes between coexisting gel and fluid phases in model membranes. *Biochim. Biophys. Acta.* 1023:25–33.

Stockton, B. W., and I. C. P. Smith. 1976. A deuterium NMR study of the condensing effect of cholesterol on egg phosphatidylcholine bilayer membranes. *Chem. Phys. Lipids.* 17:251–261.

Strandburg, K. J. 1988. Two-dimensional melting. *Rev. Mod. Physics.* 60:161–207.

Sugár, I. P., T. E. Thompson, and R. L. Biltonen. 1999. Monte Carlo simulation of two-component bilayers: DMPC/DSPC mixtures. *Biophys. J.* 76:2099–2110.

Sunamoto, J., H. Kondo, T. Nomura, and H. Okamoto. 1980. Liposomal membranes. 2. Synthesis of a novel pyrene-labeled lecithin and structural studies on liposomal bilayers. *J. Am. Chem. Soc.* 102:1146–1152.

Tardieu, A., V. Luzzati, and F. C. Reman. 1973. Structure and polymorphism of the hydrocarbon chains of lipids: a study of lecithin–water phases. *J. Mol. Biol.* 75:711–733.

Thomas, J. L., D. Holowka, B. Baird, and W. W. Webb. 1994. Large-scale co-aggregation of fluorescent lipid probes with cell surface proteins. *J. Cell Biol.* 125:795–802.

Van Dijck, P. W. M., A. J. Laper, M. A. J. Oonk, and J. de Gier. 1977. Miscibility properties of binary phosphatidylcholine mixtures. *Biochim. Biophys. Acta.* 470:58–69.

Varma, R., and S. Mayor. 1998. GPI-anchored proteins are organized in submicron domains at the cell surface. *Nature.* 394:798–801.

Vauhkonen, M., M. Sassaroli, P. Somerharju, and J. Eisinger. 1990. Dipyrenephosphatidylcholines as membrane fluidity probes. *Biophys. J.* 57:291–300.

Viola, A., S. Schroeder, Y. Sakakibara, and A. Lanzavecchia. 1999. T lymphocyte costimulation mediated by reorganization of membrane microdomains. *Science.* 283:680–682.

Vist, M. R., and J. H. Davis. 1990. Phase equilibria of cholesterol/dipalmitoylphosphatidylcholine mixtures. *Biochemistry.* 29:451–464.

Wittebort, R. J., A. Blume, T.-H. Huang, S. K. Das Gupta, and R. G. Griffin. 1982. Carbon-13 nuclear magnetic resonance investigations of phase transitions and phase equilibria in pure and mixed phospholipid bilayers. *Biochemistry.* 21:3487–3502.

Wolber, P. K., and B. S. Hudson. 1979. An analytic solution to the Förster energy transfer problem in two dimensions. *Biophys. J.* 28:197–210.

Xu, X., and E. London. 2000. The effect of sterol structure on membrane lipid domains reveals how cholesterol can induce lipid domain formation. *Biochemistry.* 39:843–849.

Zachowski, A. 1993. Phospholipids in animal eukaryotic membranes: transverse asymmetry and movement. *Biochem. J.* 294:1–14.

Zimet, D. B., B. J.-M. Thevenin, A. S. Verkman, S. B. Shohet, and J. R. Abney. 1995. Calculation of resonance energy transfer in crowded biological membranes. *Biophys. J.* 68:1592–1603.